CHEMISTRY OF MATERIALS

ARTICLE

pubs.acs.org/cm

Magnetic Core−Shell Nanoparticles from Nanoscale-Induced Phase Segregation

Sophie Carenco,[†,‡] Xavier F. Le Goff,[†] Jing Shi,[†] Lucian Roiban,[§] Ovidiu Ersen,[§] Cédric Boissière,[‡] Clément Sanchez,[*,‡] and Nicolas Mézailles[*,†]

[†]Laboratoire Hétéroéléments et Coordination, Ecole Polytechnique, CNRS, 91128 Palaiseau Cedex, France

[‡]Laboratoire de Chimie de la Matière Condensée de Paris, Collège de France, UPMC Univ Paris 06, UMR 7574 CNRS,11 place Marcelin Berthelot, 75231 Paris Cedex 05, France

[§]Institut de Physique et Chimie des Matériaux de Strasbourg, UMR 7504 CNRS−Université de Strasbourg, 23 rue du Loess, 67034 Strasbourg, France

Supporting Information

ABSTRACT: Nanoscaling of the nickel phosphides profoundly alters their domains of stability. An original mechanism of "nanoscale-induced phase segregation" was uncovered in the present study: the appearance of two crystallized phases inside each single nanoparticle (here, Ni_2P and Ni fcc), where the single-phase product (Ni_3P) would have been preferred at the bulk scale. This behavior was obtained by reacting at low temperature (<220 °C) substoichiometric amounts of white phosphorus (P_4) on well-defined monodisperse Ni nanoparticles in solution. Phosphorus insertion inside the Ni fcc nanoparticles triggers the crystallization of a Ni_2P core surrounded by a Ni shell. The crystallization process was monitored by HRTEM, EFTEM, XRD, and SQUID analyses and revealed a direct transformation of Ni fcc to a core−shell structure without any other Ni_xP_y crystallized intermediate. This core−shell Ni−P system was tuned by adjusting the amount of P_4 added, providing tunable magnetic shells supported on monodisperse nanoparticles.

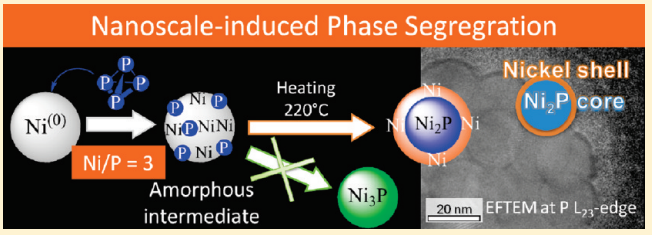

KEYWORDS: nanoscale phase segregation, core−shell nanoparticles, nanomagnetism, nickel phosphide, white phosphorus

1. INTRODUCTION

The physical properties of nanoparticles (NPs), such as their melting point or their crystallization energy, are strongly dependent on their size.[1] In particular, phase-stability domains may be deeply modified when the surface-to-volume ratio increases, leading to the appearance (or disappearance) of metastable phases and a reordering of relative stabilities.[2] Studies dealing with this problem have been mostly conducted in the case of metal oxide NPs, such as TiO_2 NPs,[3] or metal chalcogenide NPs,[4] but only a few studies deal with metal NPs.[5,6] Recent theoretical and experimental works have unraveled some of the key phenomena directing these nanoscale-induced discrepancies.[7] For instance, formation of crystalline defects can be either favored or disfavored at the nanoscale, which, in turn, alters the material's properties (such as electron transport, for example), to a great extent.[8] They can also affect the chemical reactivity, by lowering kinetic barriers for crystallization or anion/cation diffusion in the lattice.[9] Moreover, it was found very recently that phase alloying and dealloying could be promoted by H_2 reaction on the NPs surface.[10,11] All these effects are of major importance for the fine understanding of structure−property relationships.

Yet, the modifications of phase stabilities at the nanoscale have never been shown to be strong enough to induce a phase segregation within the same nanoparticle. In this article, we report, for the first time, such a nanoscale-driven transformation. The use of monodisperse nickel NPs with well-defined surface chemistry and crystallinity, as well as aging behavior, was the first prerequisite. Second, a stoichiometric and strongly reactive "P" atom donor was needed. The present mechanistic investigation of the reaction between nickel nanoparticles and low amounts of white phosphorus, P_4 (Ni/P = 3), revealed the formation of original Ni_2P−Ni core−shell spherical nanoparticles, instead of the Ni_3P nanoparticles that are expected from the stoichiometry (and known in the bulk state). This core−shell structure was shown here to result from successive amorphization and recrystallization steps inside each nanoparticle. This effect is called "nanoscale-induced phase segregation", because of the nanoscale, rearrangements occurred at low temperatures (<220 °C; note that the bulk Ni_3P and Ni_2P phases are stable up to 890 °C), which provoked a well-defined phase segregation inside each nanoparticle, in this case, the formation of a Ni_2P−Ni core−shell structure.

The course of the reaction was monitored by high-resolution transmission electron microscopy (HRTEM), X-ray diffraction (XRD), and superconducting quantum interference device

Received: February 24, 2011
Revised: March 11, 2011
Published: March 24, 2011

Scheme 1. Description of the Two Main Pathways for the Conversion of a Nickel NP to a Nickel Phosphide NP, Using White Phosphorus as a "P" Atom Donor[a]

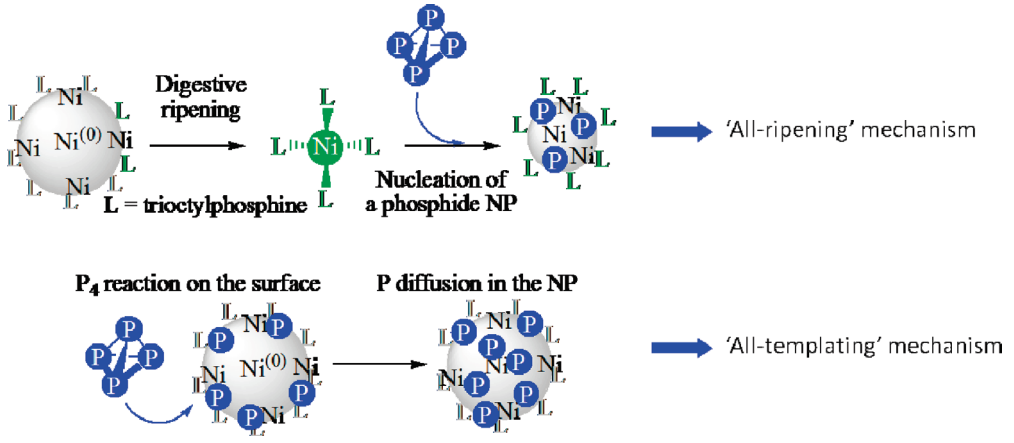

[a] Top: ripening mechanism; bottom: templating mechanism.

(SQUID) measurements at various temperatures and reaction times. The nanoscale-induced perturbation of the Ni−P material phase diagram was uncovered. Moreover, this phase segregation reaction provides monodisperse and size-controlled core−shell nanoparticles with a tunable magnetic shell, which is a rare but interesting feature for fundamental magnetic studies.[6,12]

2. RESULTS AND DISCUSSION

Metal phosphide nanoparticles have been under intensive investigation for the past 10 years, because of original properties in the fields of catalysis,[13,14] magnetism,[14,15] optics,[16] and lithium batteries.[17] Note that phosphorus doping on nickel NPs shells has been shown to be critical in the catalytic growth of TiO_2 nanotubes, by creating an active Ni−P liquid shell.[18] For nickel phosphide, common synthetic procedures use a poor P donor (an arylphosphine[19] or alkylphosphine[20]) introduced in a large excess, yielding a slow delivery of P to the metal lattice by thermal decomposition of the phosphine at a relatively high temperature (typically ~320 °C).[21] These conditions are keen to favor a slow P doping of the metal framework, along with extended diffusion abilities for both metal atoms and P atoms, because of thermal energy. Moreover, in the Ni−P system, this so-called "phosphatization" strategy allows for a certain control of the extent of reaction, giving access to various morphologies: core−shell, hollow shells, or nanowires.[22−26] In a very recent article, Tzitzios et al. described the synthesis of an original Ni−Ni_2P mixed compound, using Ni fcc NPs as a template and triphenylphosphine as a P donor at 330 °C.[27] The authors came to the conclusion that their final materials contains both Ni_2P nanocrystals and Ni hcp nanocrystals embedded in the same hollow spherical particles, based on XRD and X-ray photoelectron spectroscopy (XPS) (at Ni and P edge) measurements, even if a precise localization of each materials was not provided. However, these heating conditions jeopardize the control over the nanoparticles composition. Indeed, Omata et al. had previously highlighted that Ni fcc NPs easily convert at these temperatures to nickel carbide (Ni_3C), the XRD signature of which can be wrongly assigned to Ni hcp, because of similar lattice distances.[28] XPS analysis at the carbon edge was shown to be compulsory to distinguish Ni hcp from Ni_3C.

Therefore, it does not seem straightforward to discriminate between the formation of Ni_3C or Ni hcp in "Ni_2P−Ni" nanocomposites prepared at high temperature by the decomposition of phosphines. To exclude this possibility, a more reactive P donor was chosen, namely, white phosphorus (P_4) in a soluble form, and the room-temperature to moderate-temperature (up to 220 °C) transformations were investigated. Recently, we illustrated how easily metal nanoparticles (M = Ni, In, Pb, or Zn) react with white phosphorus (P_4), under mild conditions, to yield metal phosphide NPs, as long as the reaction is conducted in solution and with stoichiometric amounts of P.[29] We have also proved that P_4 acts as a stoichiometric P donor on Ni(0) organometallic complexes or Ni(0) nanoparticles to yield Ni_2P nanoparticles at low temperatures (<220 °C).[30] In particular, Ni_2P NPs were obtained by adding 1/8 equiv of P_4 in the solution of Ni(0) NPs, but the precise mechanism of this reaction was not elucidated at the time.

Furthermore, this preliminary study exclusively focused on the formation of the Ni_2P phase. Ni_2P is the first nickel phosphide ever obtained in the bulk scale,[31] and it is also the most stable one.[32] Even though the Ni−P phase diagram highlights the existence of many stable phases (up to 850 °C and ranging from Ni_3P to NiP_3), Ni_2P is the phase obtained in most of the cases for nanoscaled unsupported particles (<50 nm). Mixtures of $Ni_{12}P_5$ with Ni_2P or Ni(0) have also been obtained using phosphines as phosphorus donors, at intermediate times of reaction.[24] No other phase has been isolated at the nanoscale in a colloidal system so far.

2.1. Nanoscale Mechanism of the Reaction of P_4 on Ni(0) NPs. Metal insertions into a P−P bond have been largely described in organometallic chemistry.[33] A similar reaction occurs for the metal atoms on the surface of a nanoparticle stabilized by labile ligands, as we have shown in the past.[29,30] However, this does not provide insights on how a Ni(0) fcc lattice transforms, from the surface to the very core, to a Ni_2P hexagonal lattice. Two extreme pathways can be considered, as shown in Scheme 1:

(1) In an "all-ripening" process, the Ni(0) NPs serve as a reservoir for the generation of Ni(0)−TOP complexes whose structures has been described previously.[30] The nickel complexes then quantitatively react with P_4, leading to clusters that aggregate and eventually yield

dx.doi.org/10.1021/cm200575g |Chem. Mater. 2011, 23, 2270–2277

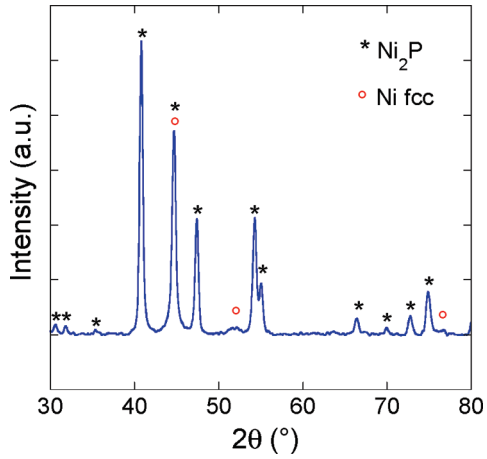

Figure 1. XRD powder — Reaction of Ni(0) monodispersed NPs with 1/12 equiv of P_4 (220 °C, 2 h).

back nanoparticles of Ni_2P. This mechanism would be favored in a large excess of phosphine and at high temperatures, which trigger ripening effects.

(2) In an "all-template" mechanism, the reaction starts on the surface (doping of the Ni lattice with P atoms) and is followed by P diffusion in the NPs. The reaction being quantitative, all the "P" atoms are accommodated in the template. In this second scenario, the size of the ending particles would be similar to that of the starting particles (with the Ni and Ni_2P structures having similar Ni atom densities).

Under phosphine-rich conditions (concentrated TOP solution, leading to a significant etching of the starting NPs), the formation of nonhollow Ni_2P NPs, smaller than the starting Ni(0) NPs, was observed by Chiang et al.[22] A competition between both mechanisms can then take place in the real reaction mixture: this is highlighted by syntheses based on the nanoscale Kirkendall effect, producing hollow NPs with intermediate ending diameters.[22,24,34]

These mechanisms have been discussed when using a poor P donor (partial decomposition of a phosphine). However, the true understanding of the lattice transformation was hampered by many features of the system: (i) the need for high temperatures (ca. 300 °C) to decompose the phosphine, which prevents a detailed study of nanocrystallization processes; (ii) an uncontrolled ripening of the NPs, because of a large excess of phosphine and high temperature; (iii) a slow delivery of P atoms on the particles, which is not properly quantified in terms of stoichiometry, along with no evidence for completeness of the reaction.

In contrast with this, our synthetic approach relies on the use of monodispersed Ni(0) nanoparticles whose surface chemistry and ripening behavior have been characterized in a previous work.[35] The NPs were systematically treated at low temperature (up to 220 °C), preventing both the decomposition of the surface ligand (TOP) and the formation of nickel carbide.[28] At 220 °C, the reaction of stoichiometric amounts of P_4 on 25-nm fcc Ni(0) nanoparticles for 2 h, a time too short to promote significant ripening, yielded quantitatively Ni_2P nanoparticles of similar diameters (see section 1 of the Supporting Information). Note that no significant dilatation of the nanoparticles was observed upon P insertion, because the number of Ni atoms per cubic nanometer is roughly the same in both structures: the Ni_2P density is higher than the Ni density. This also accounts for a stronger TEM contrast of Ni_2P, compared to Ni fcc, as will be shown in the next section. In contrast with other reported systems, our data clearly point toward a pure templating mechanism at the moderate temperature of 220 °C. This feature is readily explained by the much-higher reactivity of P_4, compared with the commonly used phosphorus sources (alkyl or arylphosphine). Indeed, the P—P bond (ca. 50 kcal/mol) is much weaker than any P—C bonds (ca. 80 kcal/mol) and all the P atoms are immediately available for the reaction with the Ni NPs, allowing a fast insertion, which we studied in detail in section 3.4 of this article.

Table 1. Size of the Crystallites and Size of the Nanoparticles for Ni NPs and Ni_2P NPs

	Scherrer size (nm)	TEM size (nm)
nickel	7.3	25
Ni_2P	23.0	25

In addition to this, a striking feature of the Ni_2P nanoparticles is their single-domain crystallinity, as evidenced by transmission electron microscopy (TEM) dark-field imaging and Scherrer evaluation of the crystallites sizes (see the Supporting Information for XRD and HRTEM analyses). Indeed, the starting Ni(0) NPs exhibited a polycrystalline fcc structure, with a typical Scherrer diameter of 7 nm (see Table 1). In addition with the P "loading" of the Ni lattice, the nanoparticles therefore underwent a complete recrystallization, without any centrifugal migration of nickel (the so-called "nanoscale Kirkendall mechanism"). Their spherical and nonfaceted shapes argue for an amorphous-like intermediate state. Related changes in terms of crystallinity have been observed using phosphines (with TOP or triphenylphosphine as a P atom donor), but, as mentioned above, under more-stringent conditions,[22,24] and were thus associated to NP morphology transformations.

Because of its shape- and size-conservative feature, this metal-to-metal-phosphide transformation could then be investigated using lower amounts of phosphorus, both from a mechanistic point of view and for the design of new composite NPs.

2.2. Core—Shell Ni_2P—Ni Nanoparticles. The reaction with a substoichiometric amount of P_4 was then studied. 1/3 equiv of P was reacted with 25-nm Ni(0) nanoparticles at 220 °C for 2 h. Logically, no free P_4 was detected by ^{31}P solution NMR at the end of the reaction, indicating its quantitative consumption. After isolation of the nanoparticles, the Ni_3P phase, expected from the initial ratio of Ni/P, was not identified but rather was a mixture of Ni_2P and Ni(0) fcc phases (see Figure 1). Interestingly, the bulk phase diagram of the Ni—P system indicates that both Ni_3P and Ni_2P phases are stable up to 890 °C.[36] This underlined a nanoscale effect on the relative phase stabilities of Ni_3P versus Ni_2P. Note in Figure 1 that the Ni fcc peaks are both weaker and broader than the Ni_2P peaks, suggesting that a significant amount of nickel could also persist in amorphous or very small crystallized domains.

These preliminary observations raised the question of the localization of both species in the sample. Indeed, the aforementioned migration of P in the Ni(0) template should also occur when one uses a substoichiometric amount of P_4, but the precise distribution of P in the NPs can hardly be predicted. Symmetry arguments plead for a "sphere-in-a-sphere" structure (with the starting NPs being spherical, and P_4 reacting homogeneously on

Scheme 2. Proposed Formation Mechanism for Ni_2P–Ni Core–Shell Nanoparticles

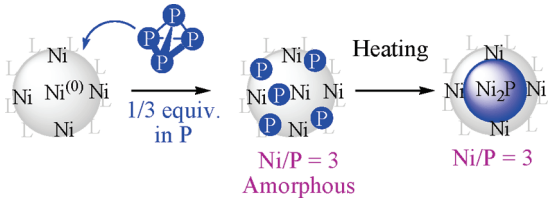

a spherical surface, the resulting NPs should have a spherical symmetry), while XRD measurements argue for larger Ni_2P and smaller Ni crystallites. On the whole, XRD analysis is compatible with nanoparticles made of a Ni_2P core surrounded by a Ni shell (see Scheme 2).

A further proof might have been given by an energy-dispersive spectroscopy (EDS) analysis of the core–shell nanocomposite. Yet, EDS studies were hampered here by (i) the presence of significant amounts of trioctylphosphine (stabilizing ligand) on the surface of the particles, and (ii) the presence of P in the core of the particles, which is only a few nanometers under the shell. Using EDS on an isolated nanoparticle of the grid, attempts at detecting significant variation of the Ni/P ratio from the outer part of a particle to its center were not successful. XPS analysis on the sample revealed significant amounts of phosphine ligands on the surface of the NPs, despite repeated washing (see the Supporting Information). Moreover, examining the Ni 2p edge spectrum gave no additional information, with the contributions of Ni(0) and Ni inside the Ni_2P structure being at the same energy. Most importantly, XPS at the C 2s edge confirmed the absence of nickel carbide (Ni_3C) in our samples, as we had anticipated under these mild heating conditions.

HRTEM observations delivered more-compelling data. They proved the formation of a core–shell structure (see Figure 2). The existence of crystallized Ni_2P domains inside the NPs, in the form of one single-crystallized Ni_2P domain in the center of each core–shell NPs, which is obvious on the HRTEM, confirmed the XRD data. The presence of a poorly crystallized Ni fcc shell (with a thickness of ca. 2 nm) around the Ni_2P core is also apparent.

In accordance with the diffusion mechanism proposed above, P atoms seem to diffuse into the nanoparticles, from the surface to the core. Phosphorus accumulates in the particles while the Ni atoms reorganize to accommodate them, resulting in crystallization of the Ni_2P structure. As a consequence, the shell is composed of the species that did not take part in the crystallization: most probably, the Ni atoms, because of the defect in stoichiometry. Assuming that all of the phosphorus would be in the core (crystallized domain), calculation indicates that the ratio of the radius core to the radius shell is $(2/3)^{1/3}$ (≈ 0.87).[37] For a 25-nm-diameter nanoparticle, the shell thickness would then be 1.6 nm, in agreement with the ca. 2 nm shell observed on the TEM pictures. Finally, energy-filtered transmission electron microscopy (EFTEM) analysis performed at the P L_{23}-edge (Figure 3) enabled us to confirm the presence of a P-poor shell, in agreement with the proposed phase-segregation mechanism. All the NPs present the same morphology, confirming the homogeneous repartition of phosphorus in the sample.

2.3. Reactivity of the Shell. As a complementary "chemical proof" for our hypothesis on the Ni-rich structure of the shell, we

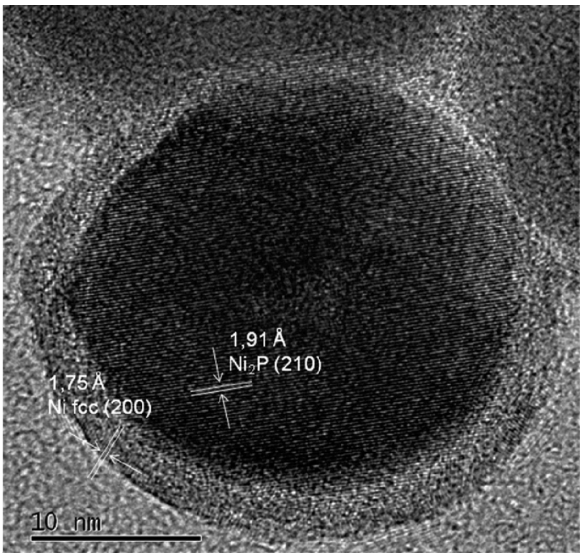

Figure 2. HRTEM observations on NPs produced by the reaction of Ni(0) NPs with 1/12 equiv of P_4 (220 °C, 2 h). The Ni_2P core appears darker than the Ni shell, because of its higher density.

Scheme 3. Reaction Pathway from Ni_2P–Ni Nanoparticles to Pure Ni_2P Nanoparticles

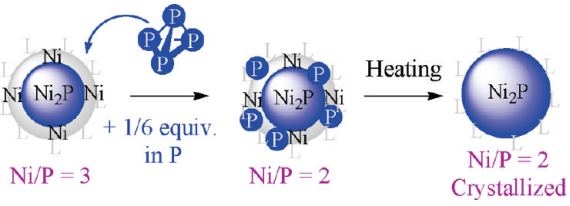

checked that reacting our Ni_2P–Ni nanoparticles with more P_4 yields pure Ni_2P nanoparticles (see Scheme 3).

The reaction was conducted without isolation of the intermediate Ni_2P–Ni core–shell nanoparticles (albeit an aliquot was taken out of the reaction mixture of XRD and TEM analyses). 1/6 equiv in P was added at room temperature to the solution of NPs, and the mixture was heated back at 220 °C for another 2 h. The analysis of the final product by XRD and TEM did indeed show the presence of pure Ni_2P nanoparticles (see the Supporting Information). This shows that the shell of the core–shell nanoparticles does indeed react as a Ni shell toward P_4, confirming its structure.

2.4. From Ni(0) NPs to Core–Shell Ni_2P–Ni Nanoparticles: A Step-by-Step Study. By heating at 220 °C for 2 h, only the crystallized Ni_2P phase could be trapped. However, we wondered if the crystallization went through an intermediate Ni_3P phase (successive phase transformation), or directly from an amorphous structure of stoichiometry Ni/P = 3 to a mixture of Ni_2P and Ni. This process was studied in detail, looking for possible metastable phases that could be trapped at lower temperatures or shorter reaction times. A first set of experiments was conducted at various temperatures (70, 120, 150, and 220 °C), and a second using different heating times (15, 30, 60, and 90 min) at 220 °C. In each case, TEM observations indicated the same size for the nanoparticles.

The experiments conducted at very low temperature (70 °C for Ni/P = 4 and 120 °C for Ni/P = 2) with a heating time of 2 h

dx.doi.org/10.1021/cm200575g |*Chem. Mater.* 2011, 23, 2270–2277

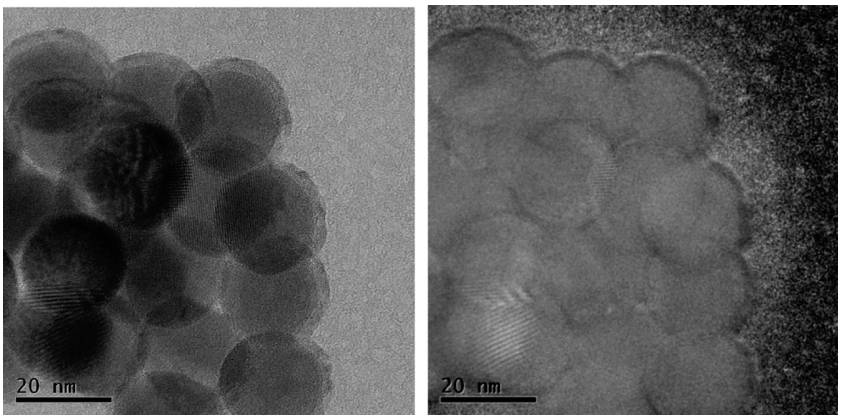

Figure 3. (Left) TEM image; (right) qualitative P-map obtained by EFTEM analysis at the P L_{23}-edge, using the jump-ratio method.

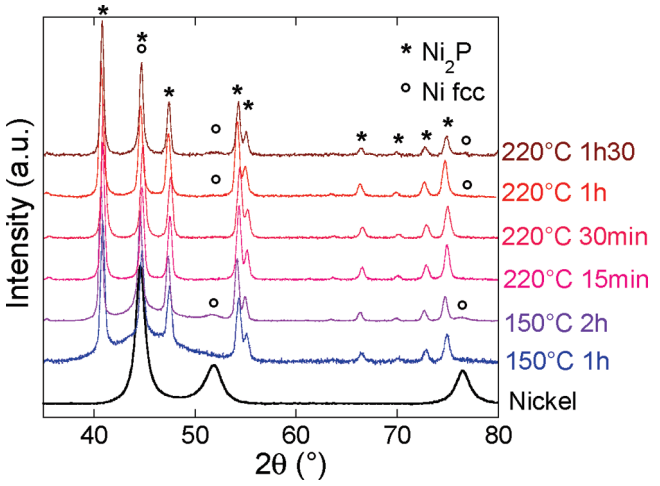

Figure 4. XRD on nanoparticles synthesized at a Ni/P ratio of 3, at different temperatures and heating times. The spectrum of the starting Ni nanoparticles is also presented, as a reference.

yielded only amorphous nanoparticles (see the Supporting Information). Only when the temperature was increased, to 150 °C, did partial crystallization (see Figure 4) of Ni_2P begin to be observed. Note that the nanoparticles were still partially amorphous nanoparticles, attested by the presence of a broad signal centered at 45° (see Figure 4). After 2 h at this temperature, Ni fcc was still detected in the sample. The second set of experiments showed that the crystallization of Ni_2P required <15 min at 220 °C. Interestingly, at this stage, no Ni fcc was observed, indicating that amorphous regions remained in the sample. Only when the heating process was extended to 90 min was partial crystallization observed via XRD (see Figure 4). This was corroborated by TEM observation of these samples (see the Supporting Information) that show the presence of a well-contrasted shell only after a long heating. The nanoscale-induced phase segregation can thus be summarized as follows: (i) the Ni_2P crystallites grow fast at 220 °C in the core of each nanoparticle, and (ii) the appearance of crystalline Ni domains is much slower. (See Scheme 4.)

No intermediate crystalline phase (Ni_3P, Ni_5P_4, $Ni_{12}P_5$) was detected during the course of the process. The system evolved according to a phase-segregation process, from a mixture of Ni and P to a well-defined Ni_2P—Ni structure.

The variation of the stoichiometry of white phosphorus vs Ni was probed, in order to tune the thickness of the shell. Analogous experiments were reproduced using Ni/P ratios of 2.5 and 4. The same steps were observed during the heating process and shell thicknesses of ca. 1.6 and 2.4 nm, respectively, were measured by TEM (see the Supporting Information).

Overall, the structure obtained here (Ni_2P in the core and Ni in the shell) is the opposite of the structure obtained in the studies reported by Zheng et al.[24a] and Wang et al.[24b] The heating conditions are softer in the present study, which could have favored the formation of the phosphide phase on the outer shell. Three points may be presented to explain our results.

(1) Migration of the Ni from the core to the shell regions of the metal phosphide is possible, as demonstrated by several reports of hollow structures from the "nanoscale Kirkendall effect".[22]

(2) The "P" atom donor, white phosphorus, because of the low P—P bond strength, is very reactive, even at low temperature. Unlike the phosphines used in the other studies, it reacts quantitatively and in a stoichiometric manner.

(3) Finally, each P_4 molecule provides 4 equiv of P atoms at a time and within the first moments of the reaction, which is a kinetically favorable process. In contrast, the decomposition of the P—C bond of the phosphines is a slow and complex mechanism: it provides only a small instantaneous amount of individual P atoms.

Overall, we believe that the core—shell structure that is observed depends on the relative kinetics of each migrating species (Ni toward the outside vs P toward the inside).

2.5. Magnetization as a Complementary Probe for Phase Segregation. The mechanism proposed in Scheme 4 involves the formation of amorphous Ni/P NPs, crystalline Ni_2P/amorphous Ni shell, and finally both crystalline Ni_2P/crystalline Ni core—shell structures. The amorphous intermediates are typically difficult to analyze, but, interestingly, crystalline Ni(0) nanoscaled domains show a magnetic contribution, while Ni_2P and Ni—P amorphous NPs do not. In order to obtain yet more-precise mechanistic information, the phase-segregation process was studied by analyzing the magnetization of the nanoparticles. The saturation magnetization of samples obtained for a Ni/P = 3 stoichiometry, heated at 220 °C for various reaction times, was thus analyzed at 5 K (see Figure 5). After the sample was cooled without any magnetic field, the magnetization was measured with

Scheme 4. Detailed Reaction Pathway from Time- and Temperature-Dependent XRD Analyses

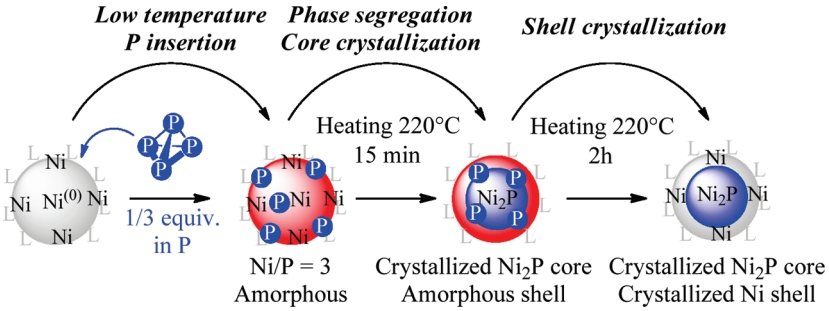

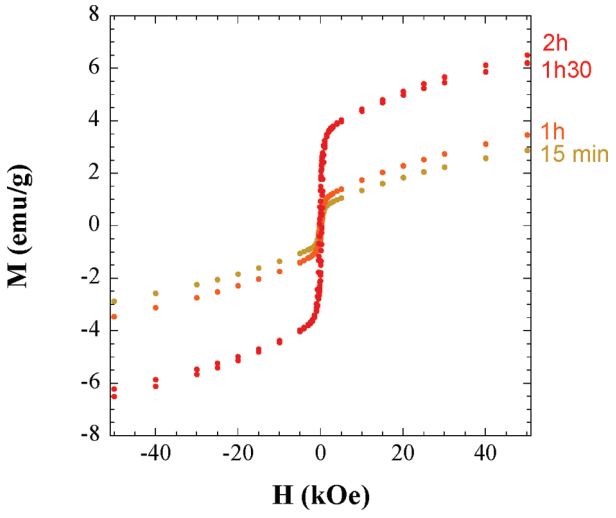

Figure 5. Magnetization−magnetic field ($M = f(H)$) curves at 5 K for Ni/P = 3 samples at different heating times.

an increasing applied field (at 5 K). Note that all the NPs have a diameter of ca. 25 nm, which is roughly the critical size for a single magnetic domain in nickel.[38] The value of saturation magnetization was larger when the sample underwent a longer thermal treatment. This proved that the appearance of a magnetization during thermal treatment was directly linked to the total amount of nickel domains that appeared in the nanoparticles. Therefore, this observation confirmed the phase-segregation mechanism shown above: starting from the amorphous phase with Ni/P ratio of 3/1, with temperature treatment, the formation of the crystalline and nonmagnetic Ni_2P core precedes the formation of crystalline nickel domains that can be magnetized.

As shown in Figure 5, the length of the thermal treatment for the process to be quantitative is ca. 2 h, in full accord with the XRD data presented above.

2.6. Ni Tunable Magnetic Shell Supported on a Ni_2P Core. Previously, it was shown that the stoichiometry of P_4 conditions the size of the Ni shell. Therefore, we postulated that it would be possible to tune the magnetic properties of the mixed Ni_2P/Ni core−shell particles by carefully adjusting the substoichiometric amount of P_4. The same reactions were conducted with various amounts of P_4 (with 2 h of heating at 220 °C) (see the Supporting Information for XRD analysis). As expected, the total magnetization was larger when the Ni(0) shell is thicker (see Figure 6). In the end, the nanoscaled phase-segregation process that takes place in every single particle could be utilized to obtain monodispersed nanoparticles with tunable saturation magnetization.

3. CONCLUSIONS

In this article, we have described an original method to prepare Ni_2P−Ni core−shell monodispersed nanocomposites under mild reaction conditions, using the fast and quantitative as well as stoichiometric reactivity of P_4 as the "P atom donor". Our study provides, for the first time, clear insights on both kinetics and thermodynamics of the formation nickel phosphide. Moreover, the reaction of substoichiometric amounts of P_4 with Ni NPs allowed us to uncover a nonclassical phase-segregation mechanism induced by the small size of the nanoparticles. The intraparticle recrystallization process starts at low temperature (150 °C), which appears to be another consequence of the nanometric size of the particles. This phase segregation from Ni_x/P_y amorphous material to a Ni_2P−Ni core shell structure was also proved using the magnetic properties of nickel. Finally, we showed that fine-tuning of the particle magnetic properties can be done via a simple variation of the P_4 substoichiometry. We believe these tunable core−shell nanoparticles, exhibiting a magnetic shell, to be of great interest for the study of magnetic interactions at the nanoscale. We are currently investigating this "nanoscaled-induced phase segregation" on more-complex systems, such as Fe−P nanoparticles, which exhibit two stable phases at the nanoscale (FeP and Fe_2P).

4. EXPERIMENTAL SECTION

Nanoparticles Synthesis. All reactions were carried out under nitrogen atmosphere, using standard air-free techniques.[39] Nickel NPs were synthesized according to a literature procedure.[35] Briefly, Ni(acac)$_2$ (2.00 g, 7.80 mmol) was added to 78.0 mmol of oleylamine (20.8 g, 10 equiv, 70% oleylamine, purchased from Aldrich) and 6.24 mmol of TOP (2.30 g, 0.8 equiv, 97% TOP, purchased from Strem). The mixture was degassed at 100 °C and heated at 220 °C for 2 h under inert atmosphere, quickly giving a black solution. After 2 h, the heating was stopped and the solution left to cool to room temperature. The Ni(0) nanoparticles solution was used as such for the second step (although a small aliquot was taken out for analysis).

Nickel phosphide nanoparticles (NPs) were obtained by adding P_4 in solution in toluene (13.0 mL; concentration in P: 0.3 mol/L, 0.5 equivalent in P) to the as-synthesized solution of nickel NPs.[40] The toluene was evaporated at 60 °C under vacuum and the solution was heated under nitrogen at 220 °C for 2 h (or at at a lower temperature or for a shorter time, as indicated in the Results and Discussion). The

dx.doi.org/10.1021/cm200575g |*Chem. Mater.* 2011, 23, 2270–2277

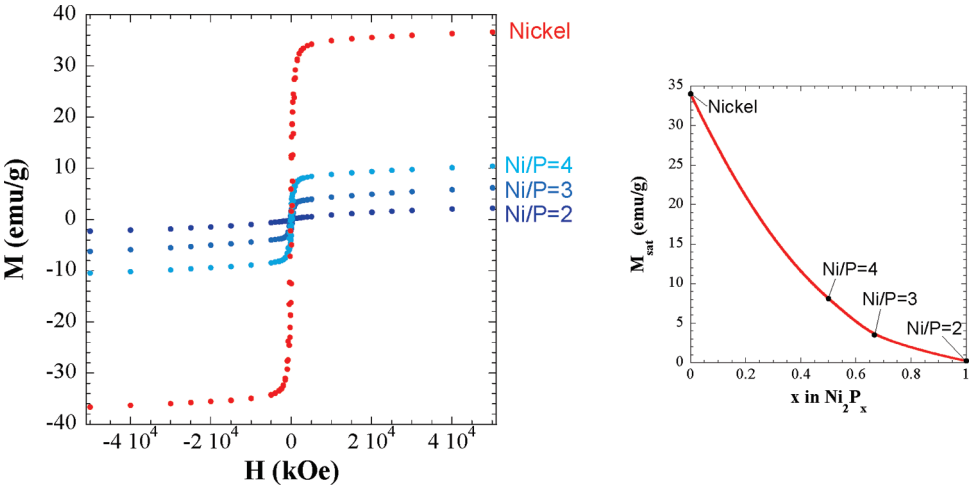

Figure 6. (Left) $M = f(H)$ curves at 5 K for Ni_xP_y NPs (thermal treatment: 220 °C, 2 h). See the Supporting Information for an enlarged view of the ±1500 kOe region. (Right) Saturation magnetization of the samples at 5 K (the line is in place to guide the eye).

mixture was cooled to room temperature and centrifuged after addition of 40 mL of acetone to give a black product. The nanoparticles could be easily redispersed in hexanes to prepare the TEM grids (deposition of one drop of the colloidal solution on a copper grid).

Other Ni/P compositions, ranging from Ni/P = 4 to Ni/P = 2, were obtained by varying the amount of P_4. The time and temperature of heating for the second step was studied, as indicated in the Results and Discussion.

Characterization. Powder XRD measurements were performed with a Bruker D8 X-ray diffractometer operating in the reflection mode, using Cu Kα radiation with a beam voltage of 40 kV and a beam current of 40 mA. The data were collected in the 20°−85° range (2θ) with steps of 0.05° and a counting time of at least 3 s.

Transmission electron microscopy (TEM) samples were prepared by evaporating a drop of a hexanes-diluted suspension of the nanoparticles on a carbon-coated copper grid. The nanoparticles were studied using a TECNAI 120 (120 kV) apparatus for routine analyses. A JEOL 2100 TEM/STEM microscope was used for HRTEM and EFTEM analyses. Qualitative P elemental maps were thus recorded in EFTEM mode at the P L_{23}-edge using the jump-ratio method.

NMR spectra were recorded on a Bruker AMX-300 spectrometer. ^{31}P chemical shifts are relative to a 85% H_3PO_4 external reference.

SQUID measurements were performed using a Cryogenic SX600 SQUID magnetometer. The measurements were recorded on very freshly synthesized nanoparticles kept under inert atmosphere. Magnetization−magnetic field ($M = f(H)$) curves were measured at 5 K. Zero field cooling (ZFC) and field cooling (FC) curves were recorded using a field of 50 G. Despite the washings, the samples contain a small fraction of organic ligands that contribute to the mass of the sample but not to the magnetization. However, the proportion of ligands is the same in all the samples. A quick calculation, based on the number of Ni surface atoms, indicates that their fraction is <5% of the total mass. Thus, the data are normalized by the mass of the nanoparticles, which includes Ni_2P and Ni, plus a very small amount of organic material.

■ ASSOCIATED CONTENT

Supporting Information. Complementary HRTEM and XRD measurements, XPS analyses on Ni_2P−Ni core−shell nanoparticles. This information is available free of charge via the Internet at http://pubs.acs.org/.

■ AUTHOR INFORMATION

Corresponding Author

*E-mails: clement.sanchez@upmc.fr (C.S.), nicolas.mezailles@polytechnique.edu (N.M.).

■ ACKNOWLEDGMENT

The research described here has been supported by Triangle de la Physique (Contract No. 2008-051T). The METSA network is acknowledged for financial support. S.C. acknowledges the DGA for financial support. C. Méthivier (LRS, UPMC, Paris) is acknowledged for the XPS measurements. Ecole Polytechnique, CNRS, and UPMC are also acknowledged for their financial support.

■ REFERENCES

(1) Zhu, Y. F.; Lian, J. S.; Jiang, Q. *J. Phys. Chem. C* **2009**, *113*, 16896.
(2) Li, Z. H.; Truhlar, D. G. *J. Am. Chem. Soc.* **2008**, *130*, 12698.
(3) (a) Zhang, H.; Banfield, J. F. *J. Mater. Chem.* **1998**, *8*, 2073. (b) Wang, C.; Ying, J. Y. *Chem. Mater.* **1999**, *11*, 3113.
(4) (a) Arachchige, I. U.; Wu, J.; Dravid, V. P.; Kanatzidis, M. G. *Adv. Mater.* **2008**, *20*, 3638. (b) Saruyama, M.; Kanehara, M.; Teranishi, T. *J. Am. Chem. Soc.* **2010**, *132*, 3280. (c) Mahler, B.; Lequeux, N.; Dubertret, B. *J. Am. Chem. Soc.* **2010**, *132*, 953.
(5) (a) Alayoglu, S.; Zavalij, P.; Eichhorn, B.; Wang, Q.; Frenkel, A. I.; Chupas, P. *ACS Nano* **2009**, *3*, 3127. (b) Delalande, M.; Marcoux, P. R.; Reiss, P.; Samson, Y. *J. Mater. Chem.* **2007**, *17*, 1579. (c) Seo, K.; Bagkar, N.; Kim, S.; In, J.; Yoon, H.; Jo, Y.; Kim, B. *Nano Lett.* **2010**, *10*, 3643.
(6) Zhang, H.; Ding, J.; Chow, G.; Ran, M.; Yi, J. *Chem. Mater.* **2009**, *21*, 5222.
(7) (a) Qi, W. H.; Lee, S. T. *J. Phys. Chem. C* **2010**, *114*, 9580. (b) Deng, L.; Hu, W.; Deng, H.; Xiao, S. *J. Phys. Chem. C* **2010**, *114*, 11026.
(8) Jiao, Y.; Zhu, H. J.; Zhou, M. J.; Wang, X. F.; Li, Q. *J. Phys. Chem. C* **2010**, *114*, 208.
(9) Park, J.; Zheng, H.; Jun, Y.; Alivisatos, A. P. *J. Am. Chem. Soc.* **2009**, *131*, 13943.
(10) Tao, F.; Grass, M. E.; Zhang, Y.; Butcher, D. R.; Aksoy, F.; Aloni, S.; Altoe, V.; Alayoglu, S.; Renzas, J. R.; Tsung, C.; Zhu, Z.; Liu, Z.; Salmeron, M.; Somorjai, G. A. *J. Am. Chem. Soc.* **2010**, *132*, 8697.

(11) Kobayashi, H.; Yamauchi, M.; Kitagawa, H.; Kubota, Y.; Kato, K.; Takata, M. *J. Am. Chem. Soc.* **2010**, *132*, 5576.
(12) Sanles-Sobrido, M.; Bañobre-López, M.; Salgueiriño, V.; Correa-Duarte, M. A.; Rodríguez-González, B.; Rivas, J.; Liz-Marzán, L. M. *J. Mater. Chem.* **2010**, *20*, 7360.
(13) (a) Oyama, S. T.; Gott, T.; Zhao, H.; Lee, Y. *Catal. Today* **2009**, *143*, 94. (b) Yao, Z.; Dong, H.; Shang, Y. *J. Alloys Compd.* **2009**, *474*, 10. (c) Li, J.; Ni, Y.; Liao, K.; Hong, J. *J. Colloid Interface Sci.* **2009**, *332*, 231.
(14) Brock, S. L.; Senevirathne, K. *J. Solid State Chem.* **2008**, *181*, 1552.
(15) Luo, F.; Su, H.; Song, W.; Wang, Z.; Yan, Z.; Yan, C. *J. Mater. Chem.* **2004**, *14*, 111.
(16) (a) Li, L.; Reiss, P. *J. Am. Chem. Soc.* **2008**, *130*, 11588. (b) Xie, R.; Battaglia, D.; Peng, X. *J. Am. Chem. Soc.* **2007**, *129*, 15432.
(17) (a) Boyanov, S.; Annou, K.; Villevieille, C.; Pelosi, M.; Zitoun, D.; Monconduit, L. *Ionics* **2007**, *14*, 183. (b) Gillot, F.; Boyanov, S.; Dupont, L.; Doublet, M. L.; Morcrette, M.; Monconduit, L.; Tarascon, J. M. *Chem. Mater.* **2005**, *17*, 6327.
(18) Kim, M. H.; Baik, J. M.; Zhang, J.; Larson, C.; Li, Y.; Stucky, G. D.; Moskovits, M.; Wodtke, A. M. *J. Phys. Chem. C* **2010**, *114*, 10697.
(19) Wang, J.; Yang, Q.; Zhang, Z.; Sun, S. *Chemistry* **2010**, *16*, 7916.
(20) Henkes, A. E.; Schaak, R. E. *Chem. Mater.* **2007**, *19*, 4234.
(21) Senevirathne, K.; Burns, A.; Bussell, M.; Brock, S. *Adv. Funct. Mater.* **2007**, *17*, 3933.
(22) Chiang, R.; Chiang, R. *Inorg. Chem.* **2007**, *46*, 369.
(23) Ni, Y.; Tao, A.; Hu, G.; Cao, X.; Wei, X.; Z. Yang, Z. *Nanotechnology* **2006**, *17*, 5013.
(24) (a) Zheng, X.; Yuan, S.; Tian, Z.; Yin, S.; He, J.; Liu, K.; Liu, L. *Chem. Mater.* **2009**, *21*, 4839. (b) Wang, J.; Johnston-Peck, A. C.; Tracy, J. B. *Chem. Mater.* **2009**, *21*, 4462.
(25) Chen, Y. *J. Cryst. Growth* **2009**, *311*, 1229.
(26) Hu, X.; Yu, J. C. *Chem. Mater.* **2008**, *20*, 6743.
(27) Zafiropoulou, I.; Papagelis, K.; Boukos, N.; Siokou, A.; Niarchos, D.; Tzitzios, V. *J. Phys. Chem. C.* **2010**, *114*, 7582.
(28) Goto, Y.; Taniguchi, K.; Omata, T.; Otsuka-Yao-Matsuo, S.; Ohashi, N.; Ueda, S.; Yoshikawa, H.; Yamashita, Y.; Oohashi, H.; Kobayashi, K. *Chem. Mater.* **2008**, *20*, 4156.
(29) Carenco, S.; Demange, M.; Shi, J.; Boissière, C.; Sanchez, C.; Le Floch, P.; Mézailles, N. *Chem. Commun.* **2010**, *46*, 5578.
(30) Carenco, S.; Resa, I.; Le Goff, X.; Le Floch, P.; Mézailles, N. *Chem. Commun.* **2008**, 2568.
(31) (a) Pelletier, B.; Pelletier, C.; Sédillot, J. *Mémoires et observations de chimie*; Chez Croullerois Librairie: Paris, 1798; Vol. 2. (b) For a review, see: Von Schnering, H. G.; Hoenle, W. *Chem. Rev.* **1988**, *88*, 243.
(32) Unpublished results obtained from DFT calculation on the Ni-P phases by J. Bernardi and M. L. Doublet; for computational details, and an extensive computational study of the metal phosphides, see: (a) Bernardi, J. Thesis, Université Montpellier, 2008. (b) Bekaert, E.; Bernardi, J.; Boyanov, S.; Monconduit, L.; Doublet, M. L.; Ménétrier, M. *J. Phys. Chem. C* **2008**, *112*, 20481. (c) Boyanov, S.; Bernardi, J.; Bekaert, E.; Ménétrier, M.; Doublet, M. L.; Monconduit, L. *Chem. Mater.* **2009**, *21*, 298.
(33) (a) Caporali, M.; Gonsalvi, L.; Rossin, A.; Peruzzini, M. *Chem. Rev.* **2010**, *110*, 4178. (b) Cossairt, B. M.; Piro, N. A.; Cummins, C. C. *Chem. Rev.* **2010**, *110*, 4164. (c) Scheer, M.; Balázs, G.; Seitz, A. *Chem. Rev.* **2010**, *110*, 4236.
(34) The nanoscaled Kirkendall effect has been described, in particular, by the pioneering work of A. P. Alivisatos. See: (a) Yin, Y.; Rioux, R. M.; Erdonmez, C. K.; Hughes, S.; Somorjai, G. A.; Alivisatos, A. P. *Science* **2004**, *304*, 711. (b) Cabot, A.; Ibáñez, M.; Guardia, P.; Alivisatos, A. P. *J. Am. Chem. Soc.* **2009**, *131*, 11326. (c) Railsback, J. G.; Johnston-Peck, A. C.; Wang, J.; Tracy, J. B. *ACS Nano* **2010**, *4*, 1913.
(35) Carenco, S.; Boissière, C.; Nicole, L.; Sanchez, C.; Le Floch, P.; Mézailles, N. *Chem. Mater.* **2010**, *22*, 1340.
(36) Okamoto, H. *J. Phase Equilib. Diffusion* **2010**, *31*, 200.
(37) The Ni density (number of Ni atoms per nm^3) is roughly the same in bulk Ni fcc and bulk Ni_2P. Therefore, we did not take any dilatation effect in consideration for the core-to-shell ratio calculation.
(38) Zhang, H. T.; Wu, G.; Chen, X. H.; Qiu, X. G. *Mater. Res. Bull.* **2006**, *41*, 495.
(39) Shriver, D. F. *The Manipulation of Air-Sensitive Compounds*, 2nd ed.; Wiley Interscience: New York, 1986.
(40) Safety Note: White phosphorus is stable in water but highly flammable and very toxic if swallowed or inhaled. It is incompatible with strong oxidizing agents and strong bases. It is light and heat-sensitive. It should be handled accordingly.